HiLumi LHC

FP7 High Luminosity Large Hadron Collider Design Study

Deliverable Report

Thermoelectrical Studies

Yang, Yifeng (University of Southampton)

22 May 2015

This work is part of HiLumi LHC Work Package **6: Cold powering**.

The electronic version of this HiLumi LHC Publication is available via the HiLumi LHC web site `<http://hilumilhc.web.cern.ch>` or on the CERN Document Server at the following URL: `<http://cds.cern.ch/search?p=CERN-ACC-2015-0052>`

Grant Agreement No: 284404

HILUMI LHC

FP7 High Luminosity Large Hadron Collider Design Study
Seventh Framework Programme, Capacities Specific Programme, Research Infrastructures,
Collaborative Project, Design Study

DELIVERABLE REPORT

THERMOELECTRICAL STUDIES

DELIVERABLE: D6.5

Document identifier:	HILUMILHC-Del-D6-5-v1.0
Due date of deliverable:	End of Month 42 (April 2015)
Report release date:	22/05/2015
Work package:	WP6: Cold Powering
Lead beneficiary:	SOTON
Document status:	Final

Abstract:

This document reports on the thermal stability studies performed on gas-cooled MgB_2 cables against local disturbances and on the filaments coupling and ac losses in conductors with a small number of filaments such as the MgB_2 wires for the SC Links. MgB_2 wires and MgB_2 cables of the type being developed for the SC Links are studied.

The information herein only reflects the views of its authors and not those of the European Commission and no warranty expressed or implied is made with regard to such information or its use.

Delivery Slip

	Name	**Partner**	**Date**
Authored by	Y. Yang	SOTON	18/05/2015
Edited by	C. Noels	CERN	18/05/2015
Reviewed by	A. Ballarino, WP6 coordinator L. Rossi, Project coordinator	CERN	22/05/2015
Approved by	Steering Committee		22/05/2015

TABLE OF CONTENTS

Executive summary

> *The report consists of two sections:*
> *1. New methods and results on the quench characteristics of laterally cooled conductors and the quench analysis of the 5kA reference cable for HL-LHC SC Links;*
> *2. Experimental studies of ac losses in 2212 round wires and implications for similarly structured MgB$_2$ round wires for HL-LHC SC Links;*

1. INTRODUCTION

Cold powering by Superconducting Links of high temperature superconducting (HTS) cable assemblies is a key technical requirement for the powering layout of the HiLumi triplets at P1 and P5. These cables, designed to work with helium gas cooling in a moderate temperature gradient between 4.2 K and 25 K, have a significantly changed cooling profile compared with low temperature superconducting (LTS) bus-bars in liquid helium. Following up on the *global* thermal-electrical models in D6.2, this report focuses on (1) the thermal stability against *local* disturbances in the presence of lateral cooling by the flow of helium gas, and (2) the filament decoupling and ac losses in conductors with small number of filaments such as the MgB$_2$ wires for the SC Links.

2. SC LINK THERMAL STABILITY

The quench behaviour of superconductors is mostly discussed in the context of winding applications, where the bulk of the conductor volume is adiabatic with cooling only at the boundaries. The LTS bus-bars in liquid helium are in the opposite situation of little quench risk as the whole conductor length is subjected to the effective lateral cooling of nucleate boiling. Cable-in-conduit conductors (CICC) with in-line supercritical helium cooling have a stability comparable to that by liquid cooling. The sub-critical helium gas cooling of the SC Links is much less potent than liquid, hence the stability against local disturbances is a valid concern and the focus of the thermal studies. Following a brief review of the existing results on the adiabatic quench analysis, we outline a new method for minimum quench energy (MQE) based on the *stationary* normal zone equations, significantly simplifying to problem to an ordinary differential equation. Furthermore, by using the uniquely simple yet profound solution for the MPZ and MQE of the critical state superconductors, a closed form analytical MQE for power-law superconductors and lateral cooling was obtained and applied for the thermal stability analysis of the SC Link.

To our knowledge such explicit results and analysis on lateral cooling do yet exist in the published literature.

2.1. LATERAL COOLING AND QUENCH CHARACTERISTICS

In the first approximation, we consider SC Links as a one dimensional linear conductor. The quench problem is represented by a well understood non-linear heat diffusion equation:

$$C(T)\frac{\partial T}{\partial x} = \frac{\partial}{\partial x}\left(k(T)\frac{\partial T}{\partial x}\right) + G(T) - H(T) \tag{1}$$

where $C(T)$ is the heat capacity *per unit volume* and $k(T)$ is the thermal conductivity. $G(T)$ and $H(T)$ are respectively the heat generation by the superconductor in the current-sharing/normal-state and lateral cooling.

2.1.1. Current Sharing Heat Generation

When the transport current exceeds the critical current due to local temperature rises, resistive heat generation follows due to partial transfer of current into the stabilisation matrix, a process known as the current sharing. For the critical state, the heat generation is given by

$$G(T) = \begin{cases} 0 & T \leq T_{cs} \\ \dfrac{\lambda^2}{1-\lambda}\rho_m(T)\big(J - J_c(T)\big)J & T_{cs} < T \leq T_c \\ \dfrac{\lambda^2}{1-\lambda}\rho_m(T)J^2 & T > T_c \end{cases} \tag{2}$$

where λ is the superconductor fill factor and $\rho_m(T)$ is the resistivity of the stabilisation matrix. With a transport current density J *per unit area of superconductor*, current sharing with the stabilisation matrix occurs at temperature above T_{cs}, where the critical current density

is reached: $J_c(T_{cs}) = J$. For superconductors with a non-linear $E(J,T)$, such as the power-law $E(J,T) = E_0 \left(\frac{J}{J_c(T)}\right)^n$, the current sharing follows a non-linear equation:

$$J = J_c(T) \left(\frac{E(J,T)}{E_0}\right)^{\frac{1}{n}} + \frac{1-\lambda}{\lambda} \frac{E(J,T)}{\rho_m(T)} \tag{3}$$

and a corresponding heat generation:

$$G(T) = \begin{cases} 0 & T \leq T_{cs} \\ \lambda J E(J,T) & T_{cs} < T \leq T_c \\ \frac{\lambda^2}{1-\lambda} \rho_m(T) J^2 & T > T_c \end{cases} \tag{4}$$

Although a closed form solution cannot be found for the current sharing equation (3) of an arbitrary n, a simple solution of $E(J,T) = \frac{\lambda}{1-\lambda} \rho_m(T)(J - J_c(T))$ for $n \to \infty$ results in the same heat generation by (4) as that of the critical state by (2).

2.1.2. Review of Adiabatic Quench Analysis for the Critical State

Classical Approach

The adiabatic quench problem, (1) with $H(T) = 0$, has been the subject of numerous studies, among which the most elegant was by Dresner [1]. The analysis starts with the approximation of small changes in the thermal-electrical properties: $C(T) = C(T_0), k(T) = k(T_0), \rho_m(T_c)$, which is justified when the transport current J is sufficiently close to the critical current $J_c(T_0)$ at the operating temperature T_0. With

$$\xi = \frac{x}{l_{MPZ}}, \qquad l_{MPZ} = \frac{\pi}{2} \sqrt{\frac{1-\lambda}{\lambda^2} \frac{k(T_0)(T_c - T_0)}{\rho_m(T) J_c(T_0) J}}$$

$$\tau = \frac{t}{t_0}, \qquad\qquad t_0 = \frac{C(T_0)}{k(T_0)} l_{MPZ}^2 \tag{5}$$

$$\theta = \frac{T - T_0}{T_c - T_0}, \qquad \theta_{cs} = 1 - j, \ j = \frac{J}{J_c(T_0)}$$

Eq (1) is transformed into a dimensionless form

$$\frac{\partial \theta}{\partial \tau} = \frac{\partial^2 \theta}{\partial \xi^2} + \left(\frac{\pi}{2}\right)^2 \frac{1-\lambda}{\lambda^2} \frac{G(\theta, J)}{\rho_m(T) J_c(T_0) J} \tag{6}$$

For the *critical state* with a critical current as a linear function of temperature, i.e,

$$J_c(T) = J_{c0} \left(1 - \frac{T}{T_c}\right) \tag{7}$$

(6) is further simplified with (2)

$$\frac{\partial \theta}{\partial \tau} = \frac{\partial^2 \theta}{\partial \xi^2} + \left(\frac{\pi}{2}\right)^2 (\theta - (1 - j)) \tag{8}$$

Dresner [1] obtained the scaling of *minimum quench energy* MQE of (7) by Lie analysis:

$$MQE \propto (1 - j)C(T_0)(T_c - T_0)l_{MPZ}A \tag{9}$$

where A is the conductor overall cross-section area. Dresner further deduced the numerical factor by solving (8) for the evolution of a Gaussian normal zone.

Recent Development of an Alternative Approach

In the present work, we report a new original development that focuses on profound properties of the critical state quench equation (8) and formulate a solution that can be generalised to power-law superconductors as well as with lateral cooling.

Dresner's MQE (8) by Lie analysis showed a current scaling of $(1 - j)j^{-0.5}$ which can be tested more readily by measurement as a function of current. It is noted that the current scaling is a more direct test for the theory than the temperature scaling which involves multiple nonlinear temperature dependences outside the usual experimental control.

With a simple transformation of

$$\theta = (1 - j)u \tag{10}$$

we point out that equation (8) is further reduced to

$$\frac{\partial u}{\partial \tau} = \frac{\partial^2 u}{\partial \xi^2} + \left(\frac{\pi}{2}\right)^2 (u - 1) \tag{11}$$

which becomes *independent of current j or J*. Notwithstanding the trivial appearance of (9), all thermal-electrical-operational parameters in the original diffusion equation (1) are eliminated. The *dimensionless MQE* of (11) is a pure number and can be obtained, as shown by Wilson [2], by minimizing the thermal energy of the *stationary* normal zone which is defined

$$\frac{d^2 u}{d\xi^2} + \left(\frac{\pi}{2}\right)^2 (u - 1) = 0, \qquad u \geq 1$$

$$\frac{\partial^2 u}{\partial \xi^2} = 0 \qquad 0 \leq u < 1 \tag{12}$$

$$u(0) = 1 + u_Q > 1 \qquad u'(0) = 0$$

The solution of (11),

$$u(\xi) = \begin{cases} 1 + u_Q \cos\left(\frac{\pi\xi}{2}\right), & |\xi| \leq 1 \\ 1 - u_Q \frac{\pi}{2}(\xi - 1), & |\xi| > 1 \end{cases}, \tag{13}$$

reveals that the current-sharing region ($u \geq 1$) of the normal zone is confined within $\xi \leq 1$. In other words the length of a critical state current-sharing section is always equal to l_{MPZ}. Note the total length of the dimensionless norm zone is $2\left(1 + \frac{2}{\pi u_Q}\right)$, which is the distance between $\pm\xi_L = \pm\left(1 + \frac{2}{\pi u_Q}\right)$ where $u(\xi_{\pm L}) = 0$. The thermal energy of the dimensionless normal zone corresponds to its integrated temperature rise:

$$\eta(u_Q) = \int_{-\xi_L}^{\xi_L} u(\xi) d\xi$$

$$= 2 \int_0^1 \left(1 + u_Q \cos\left(\frac{\pi\xi}{2}\right)\right) d\xi + 2 \int_1^{1+\frac{2}{\pi u_Q}} \left(1 - u_Q \frac{\pi}{2}(\xi - 1)\right) d\xi \tag{12}$$

$$= 2\left(1 + \frac{2}{\pi} u_Q + \frac{1}{\pi u_Q}\right).$$

At $u_Q = \frac{1}{\sqrt{2}}$, $\eta(u_Q)$ arrives at a minimum of $\frac{2}{\pi}\left(\pi + 2\sqrt{2}\right)$, which is the minimum quench energy of the dimensionless equation (10).

The thermal energy of the corresponding *dimensioned normal zone* can be obtained by returning the dimensionless solution (12) to the real space:

$$h(T_Q) = 2 \int_0^{L(T_Q)} C(T_0)(T(x) - T_0) A dx$$

$$= 2C(T_0)(T_c - T_0) l_{MPZ} A(1 - j) \int_0^{\xi_L} u(\xi) d\xi \tag{12}$$

$$= 2C(T_0)(T_c - T_0) l_{MPZ} A(1 - j) \eta(u_Q).$$

Hence the *adiabatic* minimum quench energy of 1d critical state superconductors is obtained:

$$h_{MQE} = 2C(T_0)(T_c - T_0)Al_{MPZ}(1-j)\eta_{MQE}$$

$$= (\pi + 2\sqrt{2})C(T_0)A\sqrt{\frac{1-\lambda}{\lambda^2}\frac{k(T_0)(T_c - T_0)^3}{\rho_m J_c^2(T_0)}}\frac{1-j}{\sqrt{j}} \tag{13}$$

Our MQE result (13) has the same function dependence as Dresner's MQE for a point disturbance but increases the numerical factor by $2\sqrt{2}$ (or 90% higher). In fact, the two methods give almost the same MQE when the Dresner' s correction for finite hot spots is taken into account.

It is worth noting that our method here requires only the solution of the stationary normal zone, hence significantly reduces the mathematical complexity compared with the spatial-temporal solution.

2.1.3. Quench Analysis for Power-Law Superconductors

The critical state current sharing does not adequately apply to high temperature superconductors, which typically exhibit power-law like current-voltage characteristics (CVC) resulting a greater flux motion due a short coherence length and exacerbated by thermal excitation at higher temperatures. The current-law current sharing typically results in a heat generation (3-4) which is non-linear in general as a function of temperature and in particular significantly lower in the vicinity above T_{cs}. We define a dimensionless heat generation

$$\tilde{G}(u,j,n) = \frac{1-\lambda}{\lambda^2}\frac{G(\theta,J)}{(1-j)J_c(T_0)\rho_m} = \frac{1-\lambda}{\lambda}\frac{E(j,u)}{(1-j)J_c(T_0)\rho_m}$$

$$= \frac{1-\lambda}{\lambda}\frac{1}{(1-j)e_\rho}\frac{E(j,u)}{E_0} \tag{14}$$

With a linear $J_c(T)$ as in (7), the current sharing voltage can be expressed as

$$\frac{1}{e_\rho}\frac{1-\lambda}{\lambda}\frac{E(j,u)}{E_0} = \frac{1}{e_n}\frac{E(j,u)}{E_0} = j - (1 - u(1-j))\left(\frac{E(J,T)}{E_0}\right)^{\frac{1}{n}}, \tag{15a}$$

$$e_\rho = \frac{J_c(T_0)\rho_m}{E_0}, e_n = e_\rho\frac{\lambda}{1-\lambda} \tag{15b}$$

and we have

$$\tilde{G}(u,j,n) = \begin{cases} 0 & u \leq 1 \\ (u-1) - \left(\frac{1}{1-j} - u\right)\left(\left(\frac{E(u,j)}{E_0}\right)^{\frac{1}{n}} - 1\right) & 1 < u \leq \frac{1}{1-j} \\ \frac{1}{1-j} - 1 & u > \frac{1}{1-j} \end{cases} \tag{16}$$
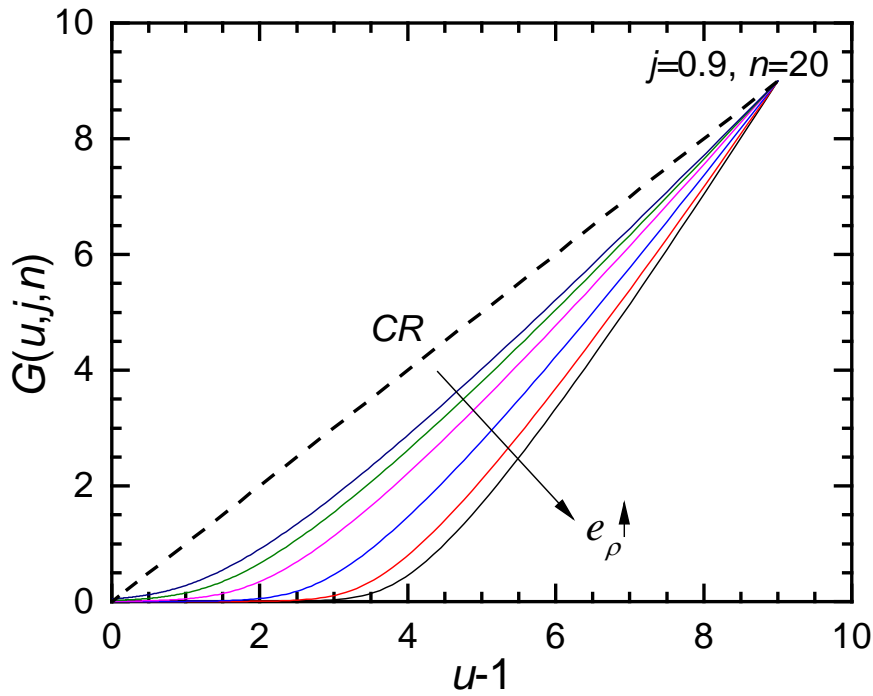
Fig 1, Non-linear current sharing heat generation of power-law superconductors as a function of temperature. The graph is an example for n=20 at j=0.9 with conductors of different normalised sheath resistance e_ρ. The linear heat generation of the critical state (CR) is shown for comparison.

The expression of $\tilde{G}(u,j,n)$ in the current sharing region $u \in \left[1, \frac{1}{1-j}\right]$ is not in a closed form as $E(u,j)$ is not explicitly obtained from (15a). However it is clear that $\tilde{G}(u,j,n)$ is *less* than the critical current sharing heat generation of $u-1$. An example of the nonlinear heat generation for power-law is shown in Fig. 1 for $j = 0.9, n = 20$ and different conductor normal resistivity given by e_ρ, the normalised full current sharing voltage (15b).

Our method of MQE for stationary equation applies readily for the power-law current sharing normal zone given by

$$\frac{d^2u}{d\xi^2} + \left(\frac{\pi}{2}\right)^2 \tilde{G}(u,j,n) = 0, \qquad u \geq 1$$

$$\frac{d^2u}{d\xi^2} = 0 \qquad 0 \leq u < 1 \qquad . \tag{17}$$

$$u(0) = 1 + u_Q > 1 \qquad u'(0) = 0$$

As numerical solutions are required, however, the results do not produce a simple expression that can clearly show the differences from the critical state.

Figure 2 shows that the nonlinear power-law heat generation $\tilde{G}(u,j,n)$ can be divided into two regimes at a point u^*: linear as $\propto (u - u^*)$ for $u > u^*$ and $\ll 1$ for $u < u^*$. Therefore $\tilde{G}(u,j,n)$ can be approximately *linearized* as

$$\tilde{G}(u,j,n) \sim \begin{cases} 0 & u \leq u^* \\ \beta^2(u - u^*) & u^* < u \leq \dfrac{1}{1-j} \\ \dfrac{j}{1-j} & u > \dfrac{1}{1-j} \end{cases} \tag{18}$$

where

$$\beta^2 = \left.\frac{\partial \tilde{G}}{\partial u}\right|_{u=\frac{1}{1-j}} = \left(je_\rho \frac{\lambda}{1-\lambda}\right)^{\frac{1}{n}} = (je_n)^{\frac{1}{n}} \tag{19a}$$

$$u^* = \frac{1}{1-j} - \frac{\tilde{G}\left(\frac{1}{1-j}, j, n\right)}{\beta^2} = \frac{1 - j\beta^{-2}}{1-j} = \frac{1 - j\left(je_\rho \frac{\lambda}{1-\lambda}\right)^{\frac{-1}{n}}}{1-j} \frac{1 - j(je_n)^{\frac{-1}{n}}}{1-j} \tag{19b}$$

are determined by linear extrapolation from $\left(\frac{1}{1-j}, \tilde{G}\left(\frac{1}{1-j}, j, n\right)\right)$ with

$$\frac{1-\lambda}{\lambda} \frac{E\left(j, \frac{1}{1-j}\right)}{E_0} = je_\rho \text{ and } \tilde{G}\left(\frac{1}{1-j}, j, n\right) = \frac{1}{(1-j)e_\rho} \frac{1-\lambda}{\lambda} \frac{E\left(j, \frac{1}{1-j}\right)}{E_0} = \frac{j}{1-j}$$
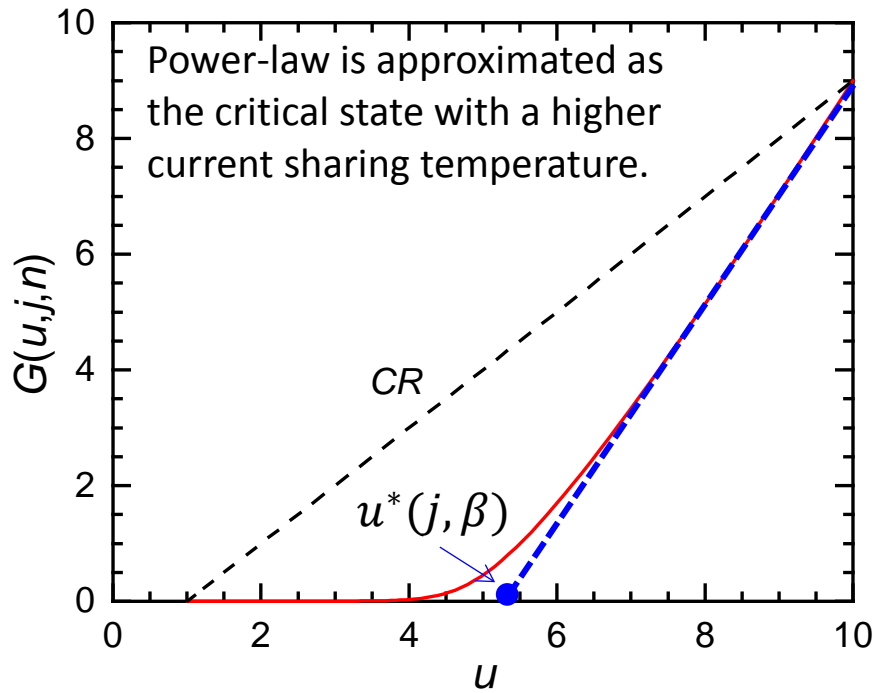

Fig 2, The non-linear heat generation of power-law current sharing can be approximately linearized as shown. The approximation effective converts a power-law superconductor to a critical state one with a high current sharing temperature.

The equations above are consistent with either J_c formulation with reference to the superconductor cross-section and the fill factor λ or the engineering current density J_e of the whole cross-section. The normalised conductor resistance is respectively defined as e_ρ and e_n. Such a linear approximation implies that the power-law current-sharing effectively increases the current sharing temperature by a factor of u^* which increases with the reduction of n and e_ρ. At $n \to \infty$, (18) is indeed returned to the critical state with $\beta = 1$ and $u^* = 1$. The linearized power-law heat generation (18) leads to the *linearization of* stationary normal zone equation (18),

$$
\begin{aligned}
\frac{d^2u}{d\xi^2} + \left(\frac{\pi}{2}\right)^2 \beta^2 (u - u^*) &= 0, \qquad u \geq u^* \\
\frac{d^2u}{d\xi^2} &= 0 \qquad\qquad 0 \leq u < u^* \\
u(0) = 1 + u_Q > 1 \qquad & u'(0) = 0
\end{aligned}
\tag{20}
$$

A further transformation by $\zeta = \beta\xi$ and $u = u^*v$ changes (17) to

$$
\begin{aligned}
\frac{d^2v}{d\zeta^2} + \left(\frac{\pi}{2}\right)^2 (v - 1) &= 0, \qquad v \geq 1 \\
\frac{d^2v}{d\zeta^2} &= 0 \qquad\qquad 0 \leq v < 1 \\
v(0) = 1 + v_Q > 1 \qquad & v'(0) = 0
\end{aligned}
\tag{21}
$$

which is identical to the critical state equation (12). Therefore equation (21) has a minimum quench energy of $\eta_{MQE} = 2\left(1 + \frac{2\sqrt{2}}{\pi}\right)$, which corresponds to a dimensioned minimum quench energy for power-law:

$$
\begin{aligned}
h_{MQE}^n &= 2C(T_0)(T_c - T_0)Al_{MPZ}(1 - j)(\beta^{-1}u^*\eta_{MQE}) \\
&= (\pi + 2\sqrt{2})C(T_0)A\sqrt{\frac{1-\lambda}{\lambda^2}\frac{k(T_0)(T_c - T_0)^3}{\rho_m J_c^2(T_0)}\frac{1 - j\beta^{-2}}{\beta\sqrt{j}}}
\end{aligned}
\tag{22}
$$

Equation (22) suggest that the power-law MQE reduces at a slower pace of $1 - j\beta^{-2}$ as $j \to 1$, of vanish at $1 - j$ in the critical state. Such a behaviour has been observed by a number of studies on HTS materials but remain unexplained prior to our analysis [3]. As an example, Fig. 3 shows that the MQE of YBCO 2G tapes agrees with the current scaling given in (22). Note the dotted lines corresponds to the $1 - j$ reduction of the critical state MQE.
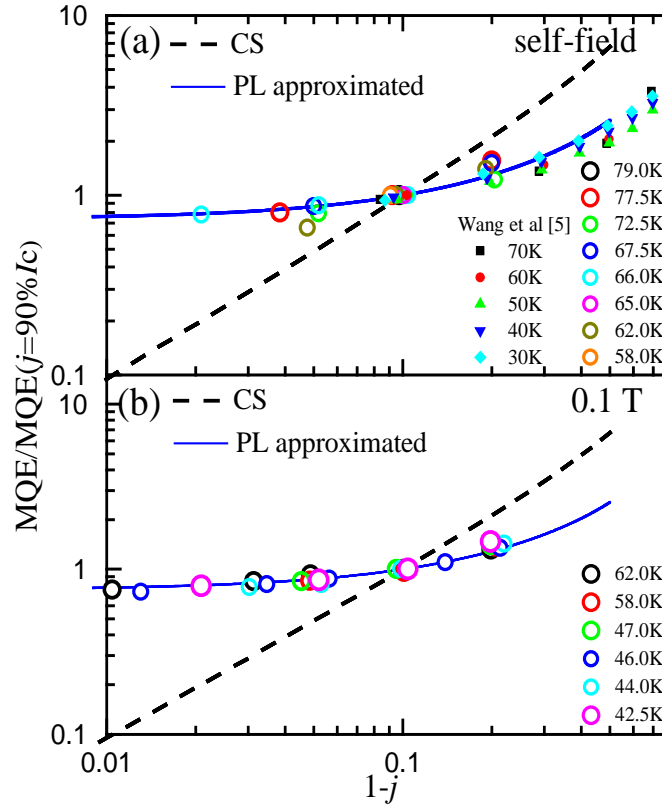
Fig 3, MQE of YBCO 2G tapes as a function of current load factor j exhibit a significant deviation from the (1-j) scaling of the critical state (dashed line). The solid lines show the prediction (22) for the power-law superconductor.

The rescaling of the length dimension in the $\zeta = \beta\xi$ in transforming the linearized approximation to an effective critical state implies a modified minimum propagation zone for a power-law superconductor, i.e., $l_{MPZ}^{n} = \beta^{-1}l_{MPZ}^{CR}$ which can become significantly longer at low current. The scaling by the increased current sharing current $u^{*} = (1 - j\beta^{-2})(1 - j)^{-1}$ points to an increased quench temperature at MPZ/MQE.

2.1.4. Quench Analysis on the Effect of Lateral Cooling

The linearization method for power-law superconductors can be readily extended to account for the lateral cooling $H(T)$ in (1). We consider lateral convective cooling by fluid at T_0:

$$H(T) = U\frac{P}{A}(T(x,t) - T_0) \qquad (23)$$

where U is the overall heat transfer coefficient including not only the convective cooling by liquid or gas cryogens around the perimeter P but also transverse/radial thermal resistances of across the conductor/cable cross-section as well as contact thermal resistances among cable strands. With the transformation (5) and (10), equation (1) becomes

$$\frac{d^2u}{d\xi^2} + \left(\frac{\pi}{2}\right)^2 \left(\tilde{G}(u,j,n) - \kappa j^{-1}u\right) = 0, \qquad u \geq 1$$

$$\left. \frac{d^2u}{d\xi^2} = \kappa j^{-1}u \qquad\qquad 0 \leq u < 1 \right. \tag{24}$$

$$u(0) = 1 + u_Q > 1 \qquad\qquad u'(0) = 0$$

where

$$\kappa = j\left(\frac{2}{\pi}\right)^2 U \frac{P}{A} \frac{l_{MPZ}^2}{k(T_0)} = \frac{1-\lambda}{\lambda_f \lambda^2} \frac{U\frac{P}{A}(T_c - T_0)}{J_c^2(T_0)\rho_m} = \frac{U\frac{P}{A}(T_c - T_0)}{\lambda_f J_e^2(T_0)\rho_n} \tag{26}$$

is introduced as the *dimensionless* **cooling number**. A further fill factor λ_f is introduced to other non-superconducting materials in the cable cross-section. Using the linear approximation for the heat generation $\tilde{G}(u,j,n)$, we have

$$\tilde{G}(u,j,n) - \kappa j^{-1}u = \beta^2(u - u^*) - \kappa j^{-1}u = (\beta^2 - \kappa j^{-1})u - \beta^2 u^* \tag{27}$$

Using a further transformation

$$\zeta = \sqrt{\beta^2 - \kappa j^{-1}}\xi, u = u_{cs}v \text{ and } u_{cs} = \frac{1}{1 - \kappa\beta^{-2}j^{-1}} u^* = \frac{1 - j\beta^{-2}}{(1 - \kappa\beta^{-2}j^{-1})(1-j)}, \tag{28}$$

and neglecting heat/cooling below u_{cs}, we have

$$\frac{d^2v}{d\zeta^2} + \left(\frac{\pi}{2}\right)^2 (v-1) = 0, \qquad v \geq 1$$

$$\left. \frac{d^2v}{d\zeta^2} = 0 \qquad\qquad 0 \leq v < 1 \right. \tag{29}$$

$$v(0) = 1 + v_Q > 1 \qquad v(0) = 0$$

Once again, (29) is identical to the critical state stationary equation (12). Hence the MQE for power-law superconductors with lateral cooling is obtained:

$$h_{MQE}^\kappa = 2C(T_0)(T_c - T_0)Al_{MPZ}(1-j)\left(\frac{u_{cs}}{\sqrt{\beta^2 - \kappa j^{-1}}}\eta_{MQE}\right)$$

$$= (\pi + 2\sqrt{2})C(T_0)A\sqrt{\frac{1-\lambda}{\lambda^2}\frac{k(T_0)(T_c - T_0)^3}{\rho_m J_c^2(T_0)}}\left(\frac{1 - j\beta^{-2}}{\beta\sqrt{j(1 - \kappa\beta^{-2}j^{-1})^3}}\right) \tag{30}$$

Now we can see that lateral cooling increases the MQE of adiabatic superconductors by a factor of
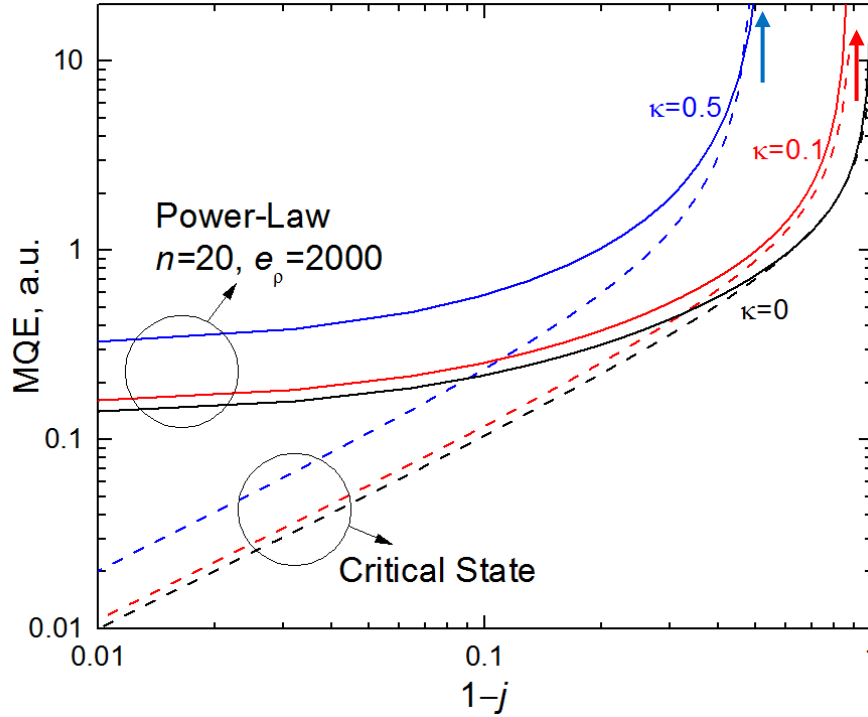
Figure 4, MQE of the critical state (dashed lines) and power-law (solid lines) as a function the current residual current load $(1 - j)$ for adiabatic $\kappa = 0$ and lateral cooled ($\kappa = 0.1$ and $\kappa = 0.5$) superconductors.

$$\frac{h_{MQE}^{\kappa}}{h_{MQE}^{n}} = \frac{1}{\sqrt{j(1 - \kappa\beta^{-2}j^{-1})^3}}, \tag{31}$$

which becomes singular at $\kappa = j\beta^2 = j(je_\rho)^{\frac{1}{n}}$ to indicate global stability at a sufficiently low current:

$$j \leq \left(\frac{\kappa}{\left(\frac{\lambda}{1-\lambda}e_\rho\right)^{\frac{1}{n}}}\right)^{\frac{n}{n+1}} \left(\frac{\kappa}{e_n^{\frac{1}{n}}}\right)^{\frac{n}{n+1}} = j_{\max} \sim \kappa . \tag{32}$$

Therefore a lateral cooled superconducting cable/bus-bar may achieve stability over local disturbances at a practical current load by increasing the heat transfer *and* by reducing overall normal resistivity. As the operating temperature approaches T_c, $j_{\max}$ tends to increase rapidly for power-law superconductors due to a vanishing $J_c(T_0)$ in e_ρ. This is *apparent* better stability at higher temperatures is the results of low current density, hence not a useful for practical application.

As expected, the presence of lateral cooling increased the stability over local disturbances by lengthening the MPZ longer at a factor of $\left((1 - \kappa\beta^{-2}j^{-1})\right)^{-1/2}$ and increasing the quench temperature at a factor of $(1 - \kappa\beta^{-2}j^{-1})^{-1}$. Fig. 4 shows the effect of cooling on the MQE for both critical state and power-law superconductors. The arrows indicate the position of $1 - j_{\max}$. In axis of the residual current load $1 - j$, the global stability is on the right of the arrow. For $j > j_{\max}$, the enhancement in MQE by lateral cooling is also present, although

useful gains still require a significant cooling number, e.g., $\kappa = 0.5$ leads to an MQE increase of 200% at $j = 0.9$ for both power-law and critical state superconductors.

2.2. CONSIDERATION FOR SC LINK WITH ENHANCED STABILITY OVER LOCAL DISTURBANCES

We now apply the quench analysis for lateral cooled superconductors to the design of superconducting bus-bars and links.

2.2.1. NbTi bus-bars in Liquid Helium

Long length NbTi ($T_c = 11K$) bus-bars in liquid helium is a useful start point due to their extensive use and proven stability in the LHC. While the Rutherford cables are typically used, their heat transfer situation is not different from a single wire. Therefore we consider a wire of diameter $d = 0.5mm$ stabilized with copper of RRR=300, i.e., $\rho_m = 5 \times 10^{-11} \Omega m$. The critical current at $T_0 = 4.2K$ is typically $J_c(T_0) = 10kAmm^{-2} = 10^{10}Am^{-2}$ at a fill-factor $\lambda = 0.25 - 0.4$. With a boiling heat transfer coefficient is $h_{\text{HeII}} = 2000 \, Wm^{-2} = U$, the cooling number κ (26) is

$$\kappa = \frac{1-\lambda}{\lambda^2} \frac{U \frac{P}{A}(T_c - T_0)}{J_c^2(T_0)\rho_m} = 4 \frac{1-\lambda}{\lambda^2} \frac{h_{\text{HeII}}(T_c - T_0)}{d \, J_c^2(T_0)\rho_m} = \begin{cases} 0.082 & \lambda = 0.4 \\ 0.26 & \lambda = 0.25 \end{cases}$$

Therefore, with the assumption of the critical state, this NbTi wire will exhibit global stability over local disturbances when operating at a current load up to 26%, i.e. $j \leq 0.26$. With a typical $E_0 = 10^{-4} Vm^{-1}$, the normalised resistance $e_\rho = 6000$. Assuming a power-law index of $n = 50$, the maximum current load is only slight reduce to $j_{\max} \sim 0.22$.

We also note that the wire diameter is an effective factor for increasing cooling number, while cladding more stabiliser to reduce the fill factor is likely to only have a linear effect as it tends to increase the overall diameters as well.

While it is desirable to have a global stability, it is also useful to assess the MQE enhancement by lateral cooling at higher current ($j > j_{\max}$), as shown below:

$$\frac{h_{MQE}^{\kappa,CR}}{h_{MQE}^{CR}} = \frac{1}{\sqrt{j(1-\kappa j^{-1})^3}} = \begin{cases} 1.9 & \lambda = 0.4 \\ 4.2 & \lambda = 0.25 \end{cases} \Bigg|_{j=0.5}$$

Therefore the MQE is increased by a factor of 4 when operating at 50% loading with a conductor of 25% fill-factor.

2.2.2. MgB$_2$ SC Links with Lateral Cooling by Subcritical Helium Gas

The MgB$_2$ SC Link for HL-LHC has a baseline wire configuration (see Fig. 5) of 0.85mm in diameter with 37 MgB$_2$ filaments. The nominal critical current at 20K is 280A, which corresponds to a wire engineering current density of $J_{e,w}(20K) \sim 500 Amm^{-2} = 5 \times 10^8 Am^{-2}$. The basic 5kA cable unit has an overall diameters of $\Phi = 6.5mm$ and consists of 18 baseline wires arranged in a single layer on the outer perimeter. Stabilising copper braids fills in the

interior of the layer of strands, therefore the effective cable engineering current is $J_{e,\Phi}(20K)\sim150Amm^{-2} = 1.5 \times 10^8 Am^{-2}$. The critical current expected and measured for the reference 5kA cable is shown in Fig. 6.

$\Phi_{wire} = 0.85$ mm
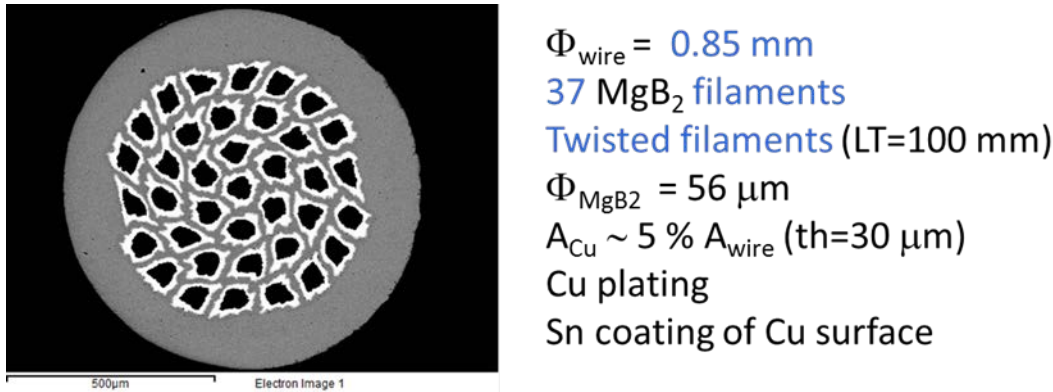37 MgB$_2$ filaments
Twisted filaments (LT=100 mm)
$\Phi_{MgB2} = 56$ μm
$A_{Cu} \sim 5 \% A_{wire}$ (th=30 μm)
Cu plating
Sn coating of Cu surface

Fig 5, The baseline MgB$_2$ wire specification for the HL-LHC SC Links.

Baseline cooling consideration and cooling number κ

We first consider cooling of the 5kA cable unit in a flexible cryostat with a nominal hydraulic diameter of $D_H \sim 10$mm. The mass flow required for the 5kA is about 0.05-0.1g/s. Hence the flow is laminar in the operating temperature range between 4.2K and 20K. Therefore the heat transfer coefficient is $h_{HeG} = 4k_{HeG}D_H^{-1} \sim 4-10 \, Wm^{-2}K^{-1} < 0.5\% \, h_{HeII}$. The thermal conductivity of helium k_{HeG} decreases from $0.026 \, Wm^{-1}K^{-1}$ at 20K to $0.01 \, Wm^{-1}K^{-1}$ at 4.2K. The the 5kA reference cable is stabilised with copper braids (RRR=300) filled at 50% inside the region enclosed by the layer of wires (Fig. 6), i.e., an effective Cu cross-section of 10mm^{-2} and a corresponding normal resistance of $\rho_n \sim 1.5 \times 10^{-10} \, \Omega m$ below 20K. The cooling number κ is
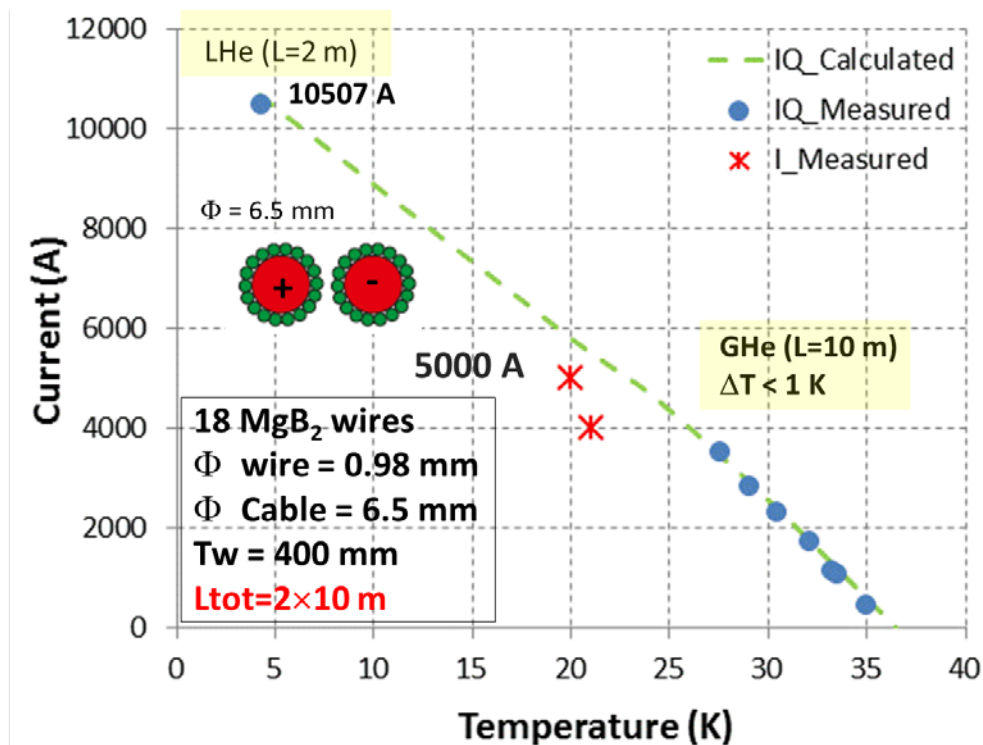

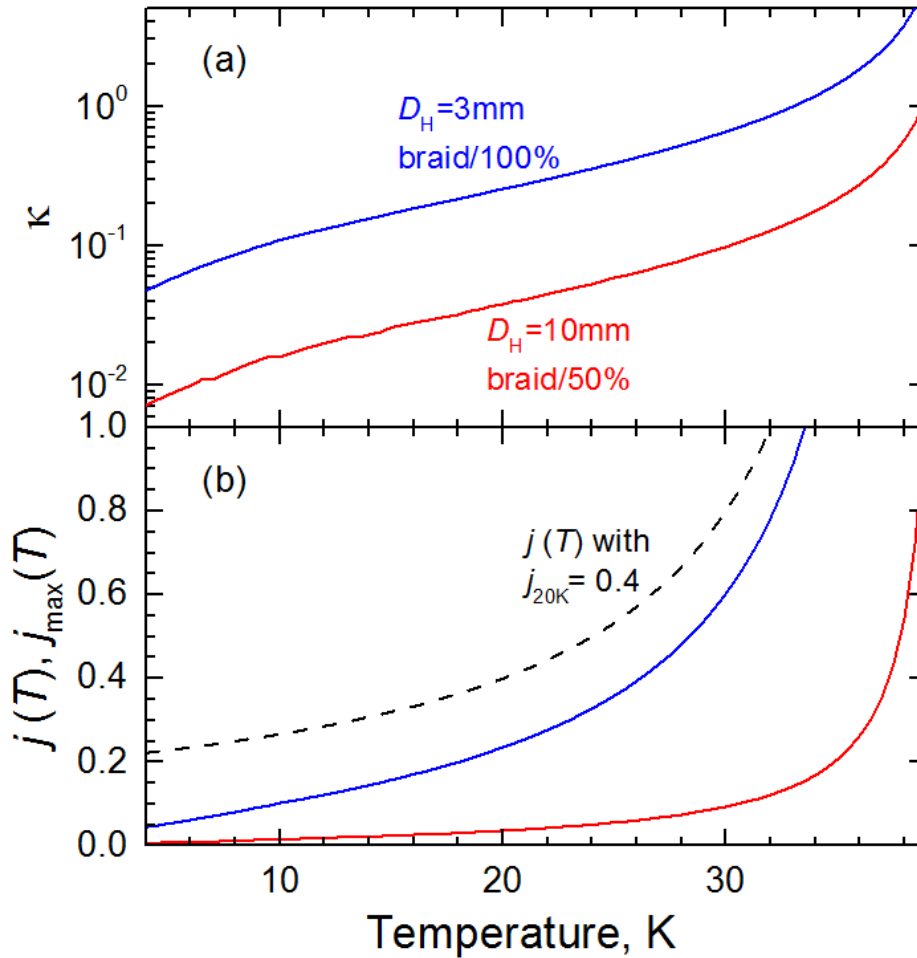*Fig 6, Critical current of the reference 5kA cable using the baseline MgB$_2$ wires [5].*

Fig. 7, (a) Cooling number κ as a function of temperature for the 5kA MgB₂ reference cable at the baseline configuration ($D_H = 10mm$ and 50% filled Cu braids) and an enhanced cooling of $D_H = 3mm$ and ~100% filled Cu braids; (b) the corresponding global stability current j_{max} with the current load $j(T)$ for $j(20K) = 0.4$ shown in comparison.

$$\kappa = \frac{U\frac{P}{A}(T_c - T_0)}{J_{e,\Phi}^2(T_0)\rho_n} = \frac{4h_{\text{HeG}}(T_c - T_0)}{\Phi J_{e\Phi}^2(T_0)\rho_n} = \begin{cases} 0.036 & T_0 = 20K \\ 0.004 & T_0 = 4.2K \end{cases}.$$

The cooling by laminar flow of helium gas in a loosely occupied cryostat is too little achieve global stability at a practical current load. It is still nevertheless important to examine whether some enhancement in stability in terms of a higher MQE can be obtained. For the SC Links, the important issue is to identify the most vulnerable region along its operating temperature gradient.

The increase of critical current and reduction of current at lower temperatures lead to a monotonous reduction of the cooling number with temperature, as shown in Fig 7(a). The cooling number (blue line Fig, 6) can be increased by 500% by increasing the fill-factor of the braid stabiliser to near 100% *and* reducing the hydraulic diameter D_H to 3mm. The latter is achievable although the implications on the cable deployment and helium pressure drop should be examined. The reduction of κ with temperature also leads to sharply lowered j_{max}, hence even the lower operating current load at low temperatures (dashed line in Fig 7(b) for
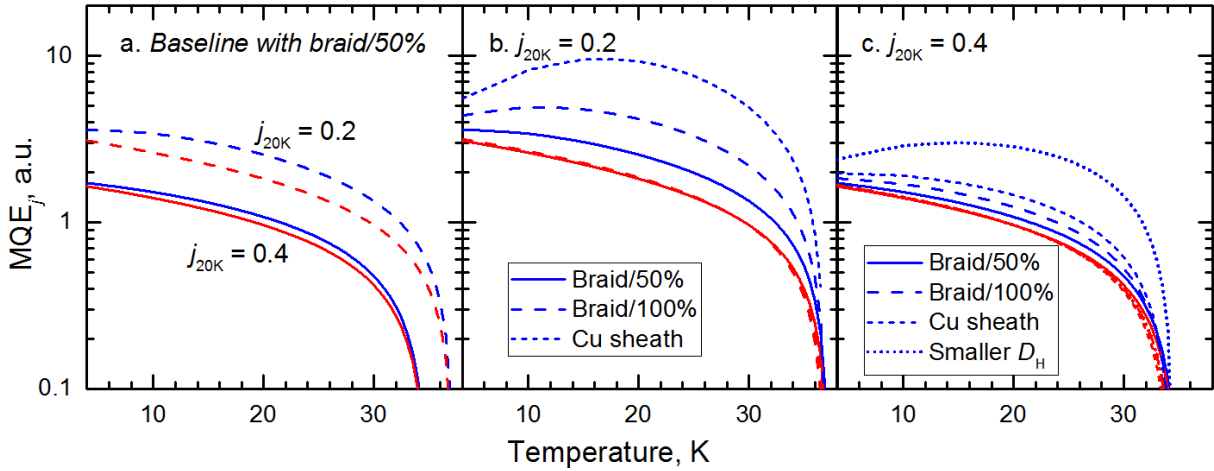
Fig. 8, MQE enhancement (blue lines) by lateral cooling for 5kA reference cable due to effect on the current scaling (MQE_J as in the parentheses of (30)) for (a) the baseline cable configuration and cooling, (b-c)by enhanced stabilisation at j(20K) = 0.2 and 0.4 respectively, and the dotted line in (c) for enhanced cooling with a reduced D_H=3mm. The adiabatic counterparts are shown in red lines for comparison.

$j(20\text{K}) = 0.4)$ cannot cross $j_{\max}$ into the global stability regime. The enhanced cooling and stabilisation brings (blue line) $j_{\max}$ considerably closer but not quite enough.

Effect of lateral cooling on MQE through changes in the current scaling

The minimum quench energy remains relevant consideration since the SC Links operate outside the global stability regime in the entire temperature range between 4K and 20K. As shown in 2.1.4, lateral cooling indeed brings MQE enhancement. The key question is whether optimisation can be made within the operational and design constraints to maximise the enhancement. The enhancement for the 5kA reference cable through the MQE scaling on the current load, shown in Fig. 8 as MQE_J vs T, corresponds to the term in the parentheses in (30) and excludes the MQE increase by a longer l_{MPZ} due to a lower ρ_n and higher k upon adding more stabilisation copper. The latter applies to both adiabatic and lateral cooled. In Fig. 8, the red lines corresponds to the adiabatic condition and blue lines for various cooling and stabilisation scenarios. Under the baseline configuration (Fig. 8(a)), lateral cooling makes little impact for the operating current of 40% loading at 20K while adding an appreciable enhancement for 20% current loading. Further increase of stabilisation materials, such as 100% fill of Cu braid (dashed) and fully copper stabilised wires (short dash) result in useful MQE increases for $j(20\text{K}) = 0.2$ (Fig. 8(b)), but still insignificant (Fig. 8(c)) for the required $j = 0.4$, which clearly demands an enhanced heat transfer by $D_H = 3$mm *and* a Cu braid filled at near 100% (dotted).

Overall MQE enhancement by lateral cooling

While the underlying mechanism for a lateral cooling enhanced MQE is by varying its current scaling, there are consequential impacts on the temperature scaling resulting further changes in the MQE. The dimensioned MQE h_{MQE} (13) obtained from $\eta_{MQE} = \frac{2}{\pi}(\pi + 2\sqrt{2})$ takes all the thermoelectric properties at constant temperature T_0. For the SC Links operating in a range of temperatures, the MQE distribution should account for several temperature effects:

- Most notably, the heat capacity falls into the cubit regime, i.e., $C(T) \propto T^3$, which leads to a sharply **lower** MQE at lower temperatures, likely to overhaul the increase in the current scaling by a reducing current load $j(T)$. Furthermore, $C(T)$ should be averaged over the temperature range of the MPZ between T and T_Q to give approximately $\bar{C}(T, T_Q) \propto (T + T_Q)(T^2 + T_Q^2)/4$. It should be noted that the lateral cooling affects T_Q through the u_{cs} transform (28), i.e., $T_Q - T = (1 - j)(T_c - T)u_Q u_{cs}$, with $u_Q^{MQE} = 1/\sqrt{2}$. All together we have

$$\bar{C}(T, T_Q) \propto \frac{1}{4}(T + T_Q)(T^2 + T_Q^2) \text{ and } T_Q = T + \frac{1}{\sqrt{2}}(T_c - T)\frac{1 - j\beta^{-2}}{(1 - \kappa\beta^{-2}j^{-1})} \quad (33)$$

- Secondly, effect of $(T_c - T_0)^{1.5}$ of an increasing temperature margin is not fully cancel by the linearly increasing critical current $J_c(T) \propto (1 - T/T_c)$, leaving a factor of $\sqrt{T_c - T}$.
- Thirdly, we have $\sqrt{k(T)/\rho_n(T)} \propto \sqrt{T}$ in the temperature regime assuming Wiedemann–Franz law $k(T)\rho_n(T) = L_o T$ with the resistivity $\rho_n(T)$ at a constant residual level.
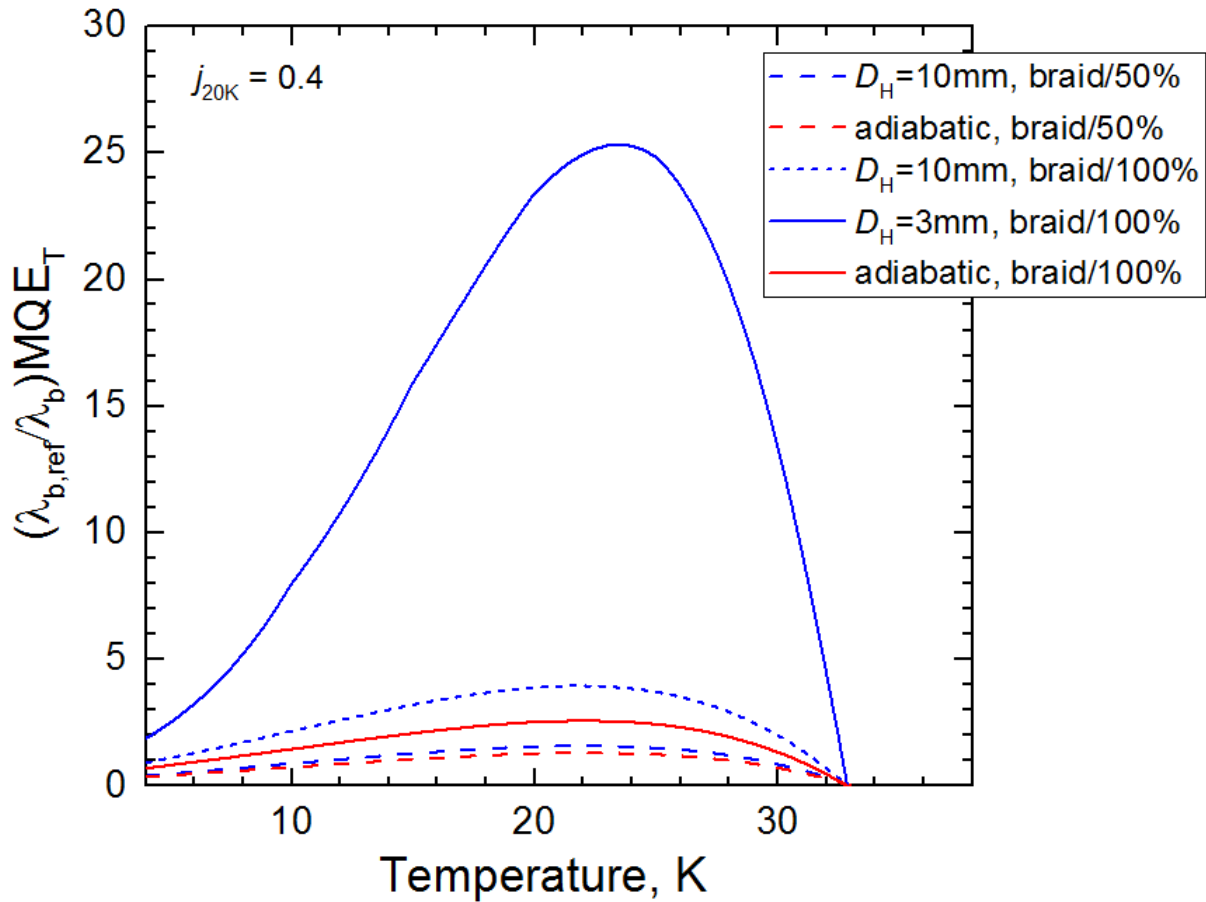

Fig. 9, The overall MQE_T of 5kA reference cable as a function of temperature for different stabilisation and cooling options.

The combined temperature scaling of the above consideration gives an overall factor

$$MQE_T = \frac{(T + T_Q)(T^2 + T_Q^2)}{4T_{ref}^3} \sqrt{\frac{T}{T_{ref}}\left(1 - \frac{T}{T_c}\right)} MQE_J$$

$$= \frac{(T + T_Q)(T^2 + T_Q^2)}{4T_{ref}^3} \sqrt{\frac{T}{T_{ref}}\left(1 - \frac{T}{T_c}\right)} \frac{1 - j(T)\beta^{-2}(j, e_n, n)}{\beta(j, e_n, n)\sqrt{j[1 - \kappa(T)\beta^{-2}(j, e_n, n)j^{-1}(T)]^3}}$$

(34)

The MQE_T in (13) is expressed as a ratio to the MQE of constant thermoelectric properties at a reference temperature T_{ref}, which could be conveniently the upper temperature of 20K for the SC Links. Fig. 9 shows distribution of the overall MQE along the 5kA reference cable along the operating temperature range between 4K and 20K. It is now clear that the overall MQE indeed reduces with temperature from 20K and the baseline lateral cooling does not make a meaningful improvement from the adiabatic condition (dashed lines). Adding more stabiliser by packing the Cu braid to near 100% lifts the MQE for both adiabatic and baseline lateral cooling (short dashed lines), the combination of $\sqrt{k/\rho_n}$ is proportional to the braid fill factor λ_b which is doubled from the reference λ_b of 50%. Furthermore, the baseline lateral cooling becomes a little more effective by adding almost 30% to the adiabatic MQE. What is more remarkable is a 500% further increase of MQE at 20K by an enhance heat transfer at a smaller $D_H = 3$mm. It is worth noting, however, that the MQE does not increase so much at 4K, where the overall MQE remains low despite a lower current load. The stability enhancement should therefore focus on the low temperature side.

2.3. FURTHER STUDIES FOR COOLING OPTIMISATION

The analysis on the lateral cooling for SC Links shows a moderate enhancement of the helium flow heat transfer coefficient can lead to a significant enhancement in the minimum quench energy MQE. The practical designs for reducing the hydraulic diameter should be considered and verified for considerations on the cable installation and overall pressure drop of the helium flow in the cryostat.

The study also highlighted that being at a lower working current load does not alter the low temperature side as the most vulnerable region for instability. Therefore it is prudent to focus on further heat transfer enhancement at low temperatures, perhaps considering the introduction local flow tubulisation.

The formulation obtained in this study can account for transverse thermal resistances, such as the conduction through the cable cross-section and contact resistances among the cable strands as well as to the stabilising matrix. Such studies should be carried out as the SC Link configurations become finalised.

Finally, the analytical results obtained here allow easier parametric verification by experimental studies, focusing on the cooling number κ.

3. UPDATES ON ELECTRICAL STUDIES OF SC LINKS

A global thermal-electrical model for Hi-Lumi SC Links has been developed within this project and reported in D6.2. The model identified that, upon the fast discharge of a 20kA circuit, a field change of 0.3T is projected in the adjacent cables in a SC Link and can cause significant magnetisation and coupling/eddy-current heating. In particular, calculations showed that fully coupled filaments pose a risk of quenching the high temperature section of the SC Links. Using the established method for superconducting wires with twisted filaments, the model further concluded that the filaments were likely to be uncoupled due to the high resistivity of the nickel matrix of the MgB_2 wire in the SC Links. Furthermore it was argued that the filaments required no special twisting as the strands of a 20kA are twisted at a pitch of 400mm hence imposing an effective length of 90mm subjected to the maximum field change as the strands move into and out of the close proximity with the discharging cable.

It was concluded in the D6.2 that additional studies should be carried to address the following issues. Firstly, there is a question about the validity of applying the ac loss calculation for large number of fine filaments to relatively small number of large filaments in the MgB_2 wires. Secondly, the calculations should be updated according to the changes in the design parameters of the wire/cable/link, including wire performance, filament architecture, materials/distribution of the stabilising matrix sub/main-cable configuration, circuit layout within the SC Links.
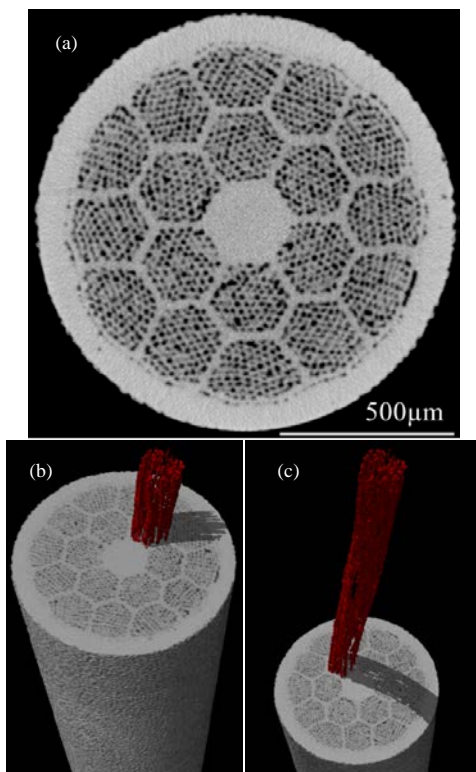

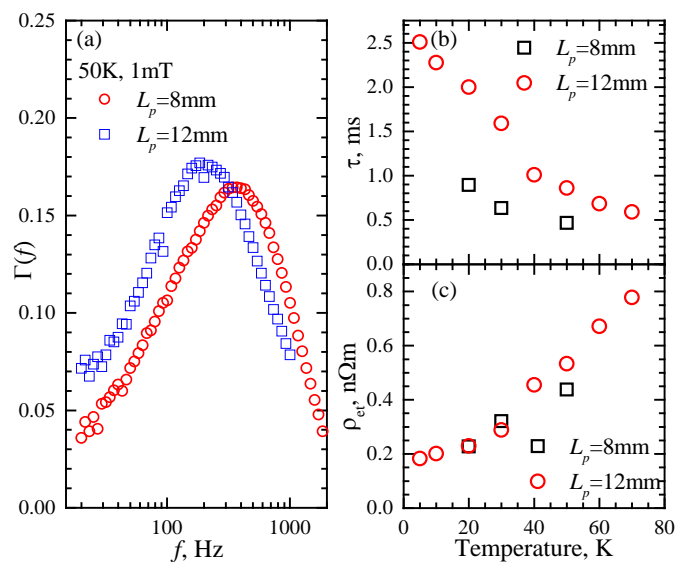*Fig. 10, Left (a-c): Architecture of a 2212 round wire with twisted filaments;*

Fig. 11, Right (a) Loss factor at 50K as a function frequency for wires at twist pitches of 8mm and 12mm. The peak corresponds to an uncoupling time constant (b) of < 1ms.

3.1. MEASUREMENTS OF AC LOSSES IN 2212 ROUND WIRES

While the ac losses of LTS conductors have been extensively studied, the uncoupling of HTS round wires at intermediate temperatures have yet to be demonstrated. With the MgB_2 round wire still undergoing intensive R&D, 2212 round wires were used as an informative substitute for experimental studies. Not only there is significant resemblance in the conductor architecture between MgB_2 and 2212 round wires, the latter also have a greater maturity in terms of performance and industrial productions. More importantly, 2212 wires with controlled filament twisting have become available from manufacturers and can be used for systematic studies of filament uncoupling in conductors with relative small number of filaments as found in MgB_2 round wires.

The 2212 wires used for the AC loss measurements has a 2-layer hexagonally restacked 2212 multifilamentary wires as shown in Fig. 11 (a). The filaments in the wires for restacking have some interconnections along the length hence are coupled in practice. On the other hand, the outer sheath of these sub-bundle wires are sufficiently thick to prevent the bridging among them after restacking and twisting. Fig. 10(b-c) shows are snapshots of X-ray tomography showing the highlighted bundle revolving 60° due to twisting.

3.1.1. Coupling Current

The frequency dependence of the loss factor is typical of that by coupling/eddy current (Fig. 10(d)):

$$\Gamma_{CP} = \lambda_f \frac{\pi z}{z^2 + 1} \text{ and } z = 2\pi f \tau_f \tag{35}$$

which has a peak value of $\Gamma_{CP}^{max} = \lambda_f \pi/2$ at $2\pi f\tau$=1 with $\lambda_f \leq 1$ being the *flux fill factor* and τ being the time constant of the coupling current. In Fig. 11(a), $\Gamma_{CP}^{max}\sim0.16$ for two different twist pitches L_p of 8mm and 12mm, suggesting a small flux fill factor of $\lambda_f\sim0.1$. A low flux fill in the restacked bundles is expected as the ac field of 1mT is too small to saturate relative restacked bundles of interconnected superconducting filaments. In the classic ac loss theory of twisted filamentary conductors, the time constant of the coupling current is determined by the
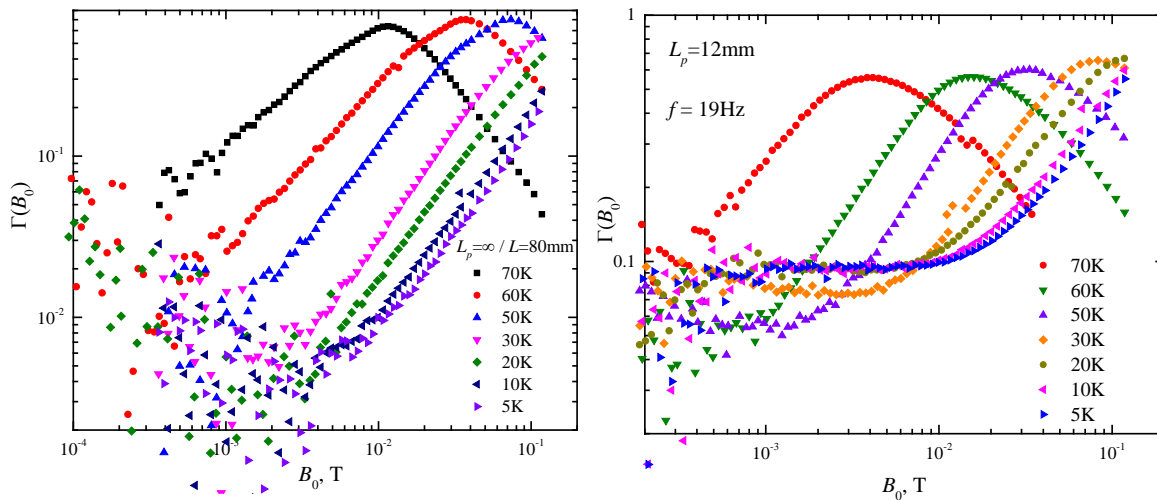

Fig. 12, Magnetisation loss factor of untwisted (left) and twisted (right, $L_p = 12mm$) at different temperatures

twist pitch and the *effective transverse* resistivity ρ_{et} across the matrix

$$\tau = \lambda_f \frac{\mu_0}{\rho_{et}} \left(\frac{L_p}{2\pi}\right)^2 = \frac{1}{2\pi f_p} \tag{36}$$

Fig. 11(a) shows that the peak position f_p shifts towards higher frequency when changing the twist pitch from 12mm to 8mm. For $L_p = 12$, the time constant at 50K is ~1ms which suggest an effective matrix resistivity of $\rho_{et}\sim0.5n\Omega m\sim0.03\rho_{cu}(300K)$. The time constant at different temperature and twist pitch were obtained as shown in Fig. 11(b). The corresponding ρ_{et}, found in Fig. 11(c), is independent of L_p and consistent with that of annealed pure silver of RRR~100. This confirms, as expected by the classical ac loss theory, that the silver matrix between the restacked bundles forms the transverse pathway of the coupling current.

Whilst confirming the validity of the classical theory for coupling current among twisted filaments, the experimental results highlight the flux fill factor as an important parameter for large filaments or restacked sub-wires/bundles.

3.1.2. Effective Diameter of Decoupling D_d

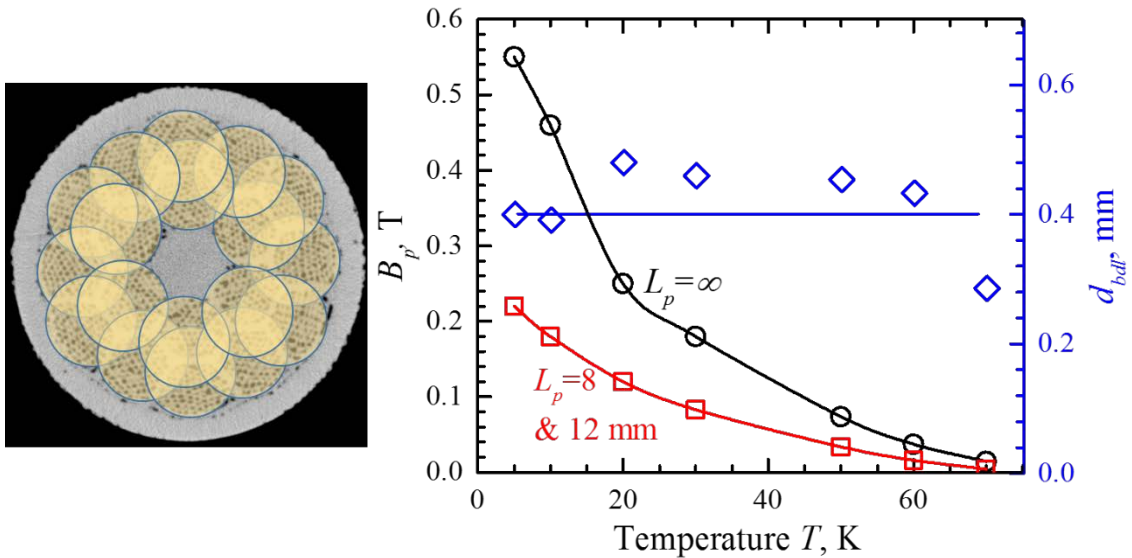While the coupling current loss is the compromise required for decoupling the filaments, the

Fig. 13, Right: Saturation field of untwisted (black circles) and twisted ($L_p = 12mm$ and $8mm$ red squares) as a function temperature. The implied diameter of decoupling (blue diamonds) is shown against the right vertical axis. Left: circles of D_h shown illustratively over the partially decoupled bundles.

effective diameter of decoupling D_d ultimately determines reduction of the magnetisation loss of the superconductor. An effective way for ascertaining D_d is measuring the magnetisation losses as a function of the ac field amplitude. The corresponding loss factor shows a peak at B_p where the decoupled bundles/filaments of D_d is saturated, i.e., $B_p\sim\mu_0 J_c D_d/2$. The experimental results on untwisted and twisted ($L_p = 12mm$) are presented respectively in the left and right panes of Fig. 12. It is evident that the saturation field of the twisted sample is consistently lower than that of the untwisted for all the temperature measured. Assuming no current degradation, since none were found between samples of 12mm and 8mm twist pitch,

the B_p ratio between twisted and untwisted conductors showed at different temperatures (Fig. 13) a consistent $D_d \sim 0.4 D_w = 1.6 D_b$, i.e., the an effective diameter of decoupling D_d about 40% of the wire diameter D_w or 1.6 times the bundle diameter D_b. Therefore the decoupling of the bundles is not complete and does not change significantly at a short pitch of 8mm. The decoupling is quite modest with D_d 60% higher than that of fully decoupled, and does change significantly with temperatures. Therefore it seems to be mainly determined by the wire architecture rather than conductor performance.

3.1.3. Further Evaluation for MgB$_2$ Wires

The updated filament configuration (Fig. 5) of the HiLumi MgB$_2$ round wires has now a 3-layer structure, packing more filaments than the number of restacked bundles in the 2212 round wires. Therefore the classical theory for couple filaments should work even better. According to the results from 2212 wires, the higher matrix resistivity of Ni/Monel in the MgB$_2$ wire should extend the uncoupling of MgB$_2$ filaments and millisecond coupling current constant to a longer twist pitch by a factor 100. Therefore there is a scope to moderating the matrix resistivity for an improved stability without compromising the filament decoupling. For example, a target twist pitch of ~100mm could become an established specification for practical MgB$_2$ round. As the baseline conductor becomes available at CERN since 2015, experimental studies similar to those on 2212 should now be carried out.

4. FUTURE PLANS / CONCLUSION / RELATION TO HL-LHC WORK

New analysis showed that lateral cooling by helium gas, although insufficient for global stability over local disturbances, can still significantly improve the MQE in SC Links when optimised. Hence experiments with controlled heat transfer conditions and design considerations for heat transfer enhancements should be carried out in the near future.

AC loss studies on 2212 round wires, architecturally similar to MgB$_2$ wires, confirmed the applicability of the classical analysis for twisted superconducting wires. The filaments in the MgB$_2$ wires should remain uncoupled over a rather long twist pitch. However the effective diameter of decoupling will be rather large, mainly determined by the filament architecture. Experimental studies on the baseline MgB$_2$ wires can now be performed as CERN as started to take deliveries from the manufacturer.

5.   REFERENCES

[1] Dresner, D. (1985) Quench Energy of Potted Magnets, *IEEE Trans Mag*, MAG-21, pp392-395.

[2] Wilson, M.N. (1983) *Superconducting Magnets*, UK: Oxford University Press

[3] Falorio, I. (2014) Quench characteristic and Minimum Quench Energy of 2G YBCO Tapes, *IEEE Trans App Supcond*, in press

[4] Morgan, G.H. (1970) Theoretical Behavior of Twisted Multicore Superconducting Wire in a Time-Varying Uniform Magnetic Field, *J. Appl. Phys.* Vol. 41, pp3673-3679

[5] First measurements of MgB_2 cables operated in helium gas up to 35 K, S. Giannelli, A. Ballarino, B. Bordini, J. Hurte,, A. Jacquemod, CERN EDMS N. 1476839

ANNEX: GLOSSARY

Acronym	Definition
LTS	Low Temperature Superconductors
HTS	High Temperature Superconductors
MQE	Minimum Quench Energy
SC	Superconducting